Nuclear Physics **A503** (1989) 473–500
North-Holland, Amsterdam

NEUTRON LIFETIME MEASUREMENT WITH A HELIUM-FILLED TIME PROJECTION CHAMBER

R. KOSSAKOWSKI[1,2], P. GRIVOT[3], P. LIAUD[1,2], K. SCHRECKENBACH[4] and G. AZUELOS[2*]

[1] *Laboratoire de Physique des Particules, BP 909, 74019 Annecy-le-Vieux, France*
[2] *Université de Savoie, BP 1104, 73011 Chambéry Cedex, France*
[3] *Institut des Sciences Nucléaires, 38026 Grenoble Cedex, France*
[4] *Institut Laue-Langevin, BP 156X, 38042 Grenoble Cedex, France*

Received 12 January 1989
(Revised 4 April 1989)

Abstract: The neutron lifetime was determined from the ratio of the neutron decay rate to the ^{3}He(n, p)t reaction rate in neutron pulses passing through a helium-filled time projection chamber. In a first experiment a value of $\tau_n = 878\ (31)$ s was obtained by this novel method.

E | RADIOACTIVITY ^{1}n; measured β^-; deduced τ_n; pulsed neutron beam; neutron decay and flux measurement in helium-filled time projection chamber.

1. Introduction

Free neutrons decay via the weak interaction semileptonic process $n \to p + e^- + \bar{\nu}_e$, with a lifetime of 15 minutes. A precise knowledge of this quantity is of major importance in particle and astrophysics.

The beta-decay lifetime τ_n is related to the axial and polar vector coupling constants g_A and g_V by

$$\tau_n \propto (g_V^2 + 3g_A^2)^{-1} . \tag{1}$$

In combination with g_A/g_V, obtained from beta-decay asymmetry measurements of polarized neutrons [1]), the lifetime measurement allows, therefore, a determination of the individual coupling constants. Hence, the value of the Cabibbo angle can be derived. This should be in principle the best method of determining these parameters, since it is independent of nuclear physics, although at present higher precision is obtained using the value of g_V from Fermi superallowed beta transitions [2]). Nevertheless, the degree of consistency of all the data tests CVC and PCAC theories, and the universality of the weak interaction.

* On leave from TRIUMF, Vancouver BC, V6T2A3, Canada.

The inverse reaction to the neutron decay, $\bar{\nu}_e + p \rightarrow n + e^+$, is commonly used to detect electron antineutrinos. The cross section of this reaction is proportional to τ_n^{-1} and depends on the helicity purity of electron antineutrinos [3]). Recent neutrino oscillation experiments illustrated the importance of a normalization by using τ_n, in order to search for a possible deficit of the event rate in the neutrino detector [4]).

In astrophysics the hydrogen burning in the sun $p + p \rightarrow d + \nu_e + e^+$ is proportional to g_A^2 and the solar neutrino flux as well as the ratio of the abundances ^{4}He to ^{1}H in the early universe depends on the neutron lifetime [5]).

At present the most precise direct measurements of τ_n report an accuracy of about 1%, but differ among each other as much as 7%, although more consistency can be observed among recent experiments [6-12]) (see fig. 1).

Direct measurements of τ_n can be classified as:

(i) storage experiments using ultra-cold neutrons in material or magnetic neutron bottles. Recent developments work towards a better control and reduction of the wall losses in the bottle [9,11,12]);

(ii) in-beam measurements of the decay products (electrons and/or protons). Recently chopped beams were used for this method [10,13]).

In the present work an experiment using the method (ii) is outlined. The experimental difficulties in this type of method reside in a precise determination of the neutron flux density and in an efficient detection of the full spectrum of the decay electrons (end point 782 keV) or of the protons (end point 0.75 keV). In previous works, separate devices were used for detection of the decay products and for flux

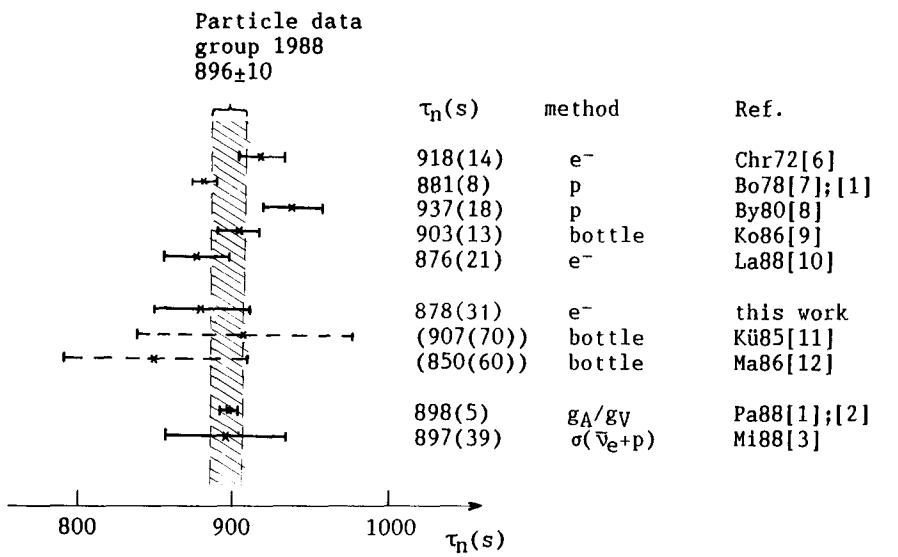

Fig. 1. Available data on the neutron lifetime. The particle-data group adopted the average of the first five measurements. The values of refs. [11,12]) are the first results, more precise data are forthcoming. The values from g_A/g_V and the cross-section measurement $\bar{\nu}_e + p \rightarrow n + e^+$ are evaluated under the assumption of CVC and no $\bar{\nu}_e$ oscillation or right-handed currents, respectively.

measurements. In our approach, a chopped neutron beam was used, and the ratio of the decay-electrons rate to the neutron density was determined simultaneously with the same apparatus. This ratio yields directly the neutron lifetime.

2. Principle of the experiment

The basic layout of the experiment is illustrated in fig. 2. Cold neutrons exit from a primary neutron guide. A rotating drum serves as a double chopper and forms neutron packets. The beam is monochromatized by a graphite crystal in order to limit the spatial spread of the packets during their flight path. The 90° deflection out of the main neutron beam provides favourable background conditions.

The neutron packets pass through a secondary guide and enter a $He+CO_2$-filled drift chamber which works in the time projection mode. A ^6LiF beam stopper finally absorbs the neutron bursts.

During a time interval Δt, the entire neutron packet moves inside the drift volume and the number of decay electrons ΔN_e is detected in a 4π geometry. The decay constant $\lambda_n = \tau_n^{-1}$ is given as

$$\lambda_n = \frac{1}{N}\left(\frac{\Delta N_e}{\Delta t}\right). \tag{2}$$

The number N of neutrons in the packet is evaluated by observing, simultaneously to the decay electrons, the products of the $^3He(n, p)t$ reaction in the drift chamber. For this purpose a small, well defined quantity of ^3He is admixed to the counter gas (see sect. 5). The decay electron and (n, p) events can be well discriminated due to their very different ionization power in the detector gas. By this method the neutron decay and neutron density are measured simultaneously in the same detector and provide a direct measure for the neutron lifetime.

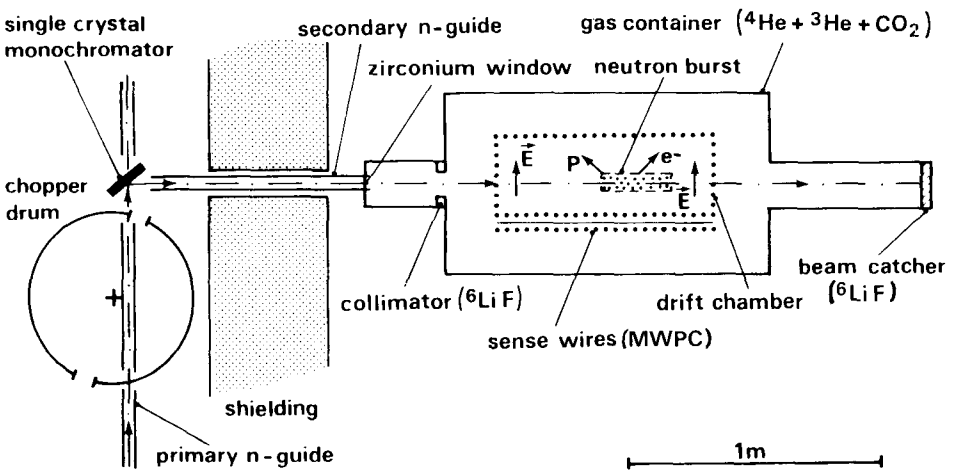

Fig. 2. Schematic view of the experimental setup. Only a part of the radiation shielding is shown.

The number of ^{3}He(n, p)t reactions in the time interval Δt is given by

$$\Delta N_{p_0} = \int \frac{dN}{dv} \rho_0 \Delta l(v) \sigma(v)\, dv, \tag{3}$$

where ρ_0 is the number of ^{3}He atoms per unit of detector volume; $\Delta l(v)$ the path length of a neutron of velocity v in a time interval Δt; $\sigma(v)$ the (n, p) cross section of ^{3}He; and dN/dv the velocity distribution in the neutron packet.

With

$$\Delta l(v) = v\Delta t, \qquad \sigma(v) = \sigma_0 \frac{v_0}{v}, \tag{4}$$

the eqs. (2)-(4) lead to

$$\lambda_n = \left(\frac{\Delta N_e}{\Delta N_{p_0}}\right) \rho_0 \sigma(v_0) v_0 . \tag{5}$$

The (n, p) cross section of ^{3}He is well known as 5333 ± 7 b at $v_0 = 2200$ m/s [ref. [14])], and the $1/v$ dependence of the cross section is well established for the present neutron velocity range [15]).

Thus, the measurement is independent of the velocity of the neutrons and the knowledge of the absolute neutron flux. Due to the simultaneous measurement of the neutron flux and decay only a second-order dead time correction of the detector system is necessary (see the appendix).

It is reduced to the determination of the ratio of decay electrons to ^{3}He(n, p)t events and the measurement of the ^{3}He content in the counter gas. The events occur inside of the counter gas and can be recorded with 100% efficiency. In contrast to solid-state detectors used previously for decay-electron detection the energy cutoff in the counter gas can be set very low and thus essentially the whole decay-electron spectrum is recorded. On the other hand the beam passes directly through the counter gas and the detector has a large volume. These facts demand a careful reduction of the background.

In the following the individual parts of the experimental setup are described. Details to the drift chamber itself were already given in ref. [16]).

3. The pulsed neutron beam

The cold-neutron beam from the primary neutron guide was collimated by a ^{6}LiF diaphragm to a cross section of 15×25 mm^2 before entering the rotating chopper drum. The initial neutron spectrum is shown in fig. 3. The drum had a diameter of 50 cm and its axis was displaced by 3 cm relative to the neutron beam axis. Two opposite slits of 25 mm were cut in the B_4C coated drum walls. At a rotation frequency of 3300 turn/min. the time-of-flight of neutrons for the 50 cm distance between the two slits and the displacement of the slits in this time interval are

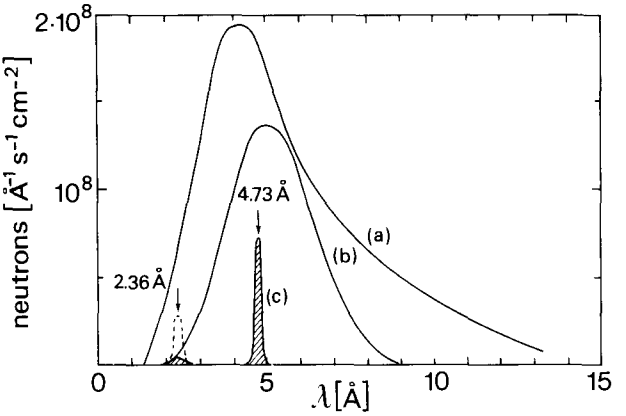

Fig. 3. Wavelength spectrum of the neutrons at different points of the beam line. (a) Exit of main guide, (b) exit of chopper drum, (c) secondary beam. The first and the second-order Bragg reflection lines are indicated (4.73 and 2.36 Å, respectively). The intensity of the 2.36 Å line, strongly reduced by the velocity preselection of the chopper drum, is not on scale and is in fact only 0.4% of the intensity of the first-order reflection. The dashed line shows the intensity of this 2.36 Å line without the attenuation.

synchronized for neutrons of ~5 Å wavelength. The wavelength resolution $\Delta\lambda/\lambda$ was about 35% (fig. 3). A neutron guide section was placed inside of the chopper. Since the two slits cut the neutron beam from opposite directions, a symmetric pulse profile is formed.

The chopped and poorly monochromatic beam was then irradiating a graphite monochromator. A 90° Bragg reflection at the [001] plane of graphite produced the secondary beam of a wavelength of 4.73 Å corresponding to the first-order reflection. The neutron intensity from the second-order reflection at 2.36 Å was only 0.4% of that from the first order due to the premonochromatization by the chopper drum (see fig. 3).

Because of the rather large mosaicity of the monochromator (1.2°), the wavelength resolution was mainly given by the divergency of the beam, defined by the cutoff angle ϕ_c for reflection of 4.7 Å neutrons in the Ni-coated neutron guides.

$$\Delta\lambda/\lambda = \operatorname{ctg}\theta\ \Delta\theta, \qquad \Delta\theta = \pm\phi_c \tag{6}$$

For our case with Bragg angle $\theta = 45°$, $\phi_c(4.7\ \text{Å}, \text{Ni}) = 0.008$ rad the wavelength resolution was 0.8%. The reflectivity of the crystal was measured as 0.5 at 4.7 Å.

After the deflection the neutron pulse entered into the secondary neutron guide of 120 cm length and $15 \times 25\ \text{mm}^2$ cross section. Both, the chopper drum and the secondary guide were filled with helium to limit the diffusion of neutrons. The neutrons passed then the 25 μm zirconium entrance window of the drift chamber and were finally absorbed in the ^{6}LiF beam catcher. A ^{6}LiF diaphragm was placed in front of the drift volume to absorb the halo of the neutron beam.

The repetition rate of the neutron pulses was chosen so that only one pulse was in the secondary beam line at a time and the primary beam was closed by the

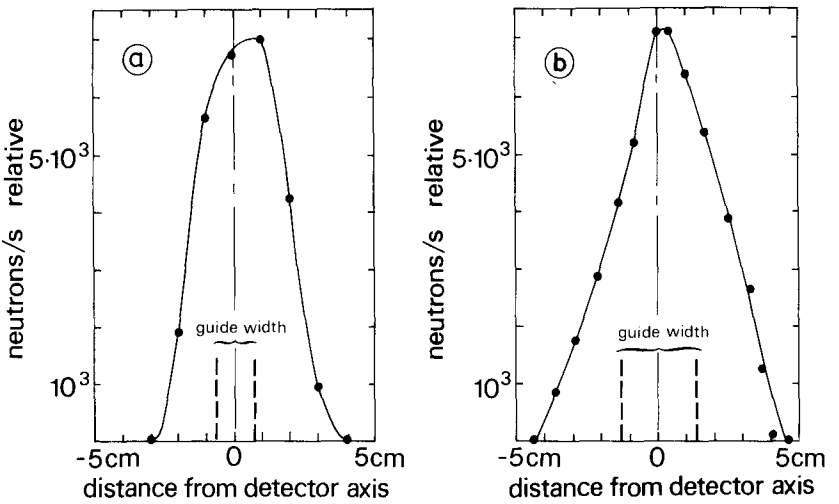

Fig. 4. Neutron beam profile measured at the site of the beam catcher. The size of the secondary neutron guide is indicated. (a) Horizontal direction, (b) vertical direction.

chopper drum during this period. With this timing the background from the primary beam was kept very low (see sect. 6).

The following beam characteristics were finally achieved:

- neutron wavelength: $\lambda = 4.73$ Å
- resolution: $\Delta\lambda/\lambda = 0.8\%$.
- length of the pulse: 23 to 25 cm
- neutrons per pulse: 2000
- neutrons at the second order of reflection (2.36 Å): 0.4% of the first order
- repetition rate of pulses: 110 per s
- divergence of the beam: $\pm 0.5°$.

In fig. 4a, b the measured beam profile at the position of the beam catcher are given.

Alternatively, an attempt was made to use a second chopper, 350 cm upstream of the chopper drum and synchronized with it. The graphite monochromator was removed, and the detector put directly in the primary beam. With this arrangement about five times more neutrons per pulse were counted, but the level and time structure of the background was not favourable for a precise measurement.

4. The time projection chamber

The tracks and ionisation power of the decay electrons and ^{3}He(n, p)t reaction products were detected in a drift chamber of 70 cm length, working in the time projection mode. A detailed description of this device is given in ref. [16]).

Fig. 5 shows a schematic view of the detector. The neutron pulse moves along the axis of the drift volume through the counter gas. A gas mixture of low neutron capture and scattering cross section had to be chosen [17]). We adopted a mixture of

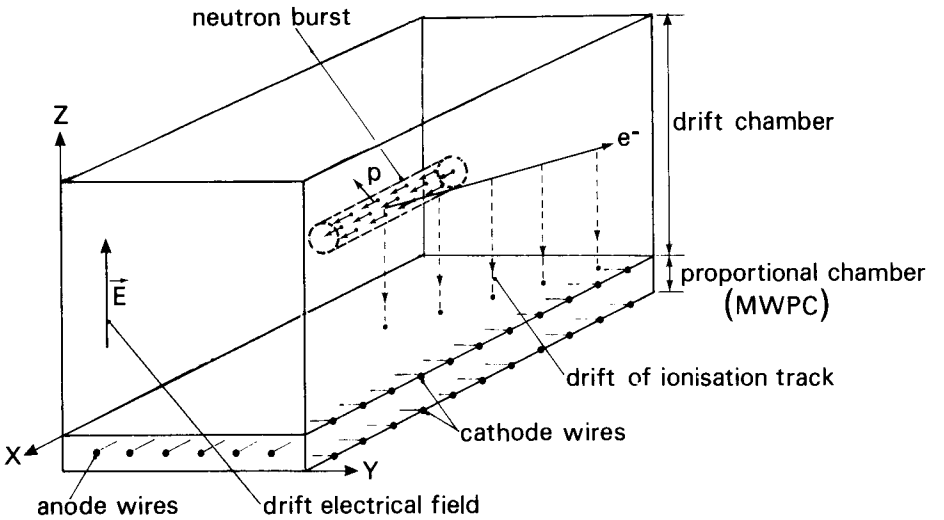

Fig. 5. Schematic view of the drift chamber. The neutron bursts move through the center of the drift volume along the x-axis.

93% He + 7% CO_2, where the dominant component ^{4}He has a low neutron scattering cross section of 1 b at 5 Å and is the only isotope with a zero neutron capture cross section. The quenching gas CO_2 does also not affect the neutron beam in a perceptible way. The total gas pressure was 950 mbar.

For gas filling the aluminium vessel which contained the drift chamber was evacuated and purged with ^{4}He. The He gas was passed through a liquid helium cooled baffle to retain nitrogen and other impurities.

An ionization track in the counter gas is drifted by the applied electrical field with a speed of about 1 cm/μs towards the multiwire proportional chamber (MWPC) section. The crossed anode-cathode wires detect the projection in the xy plane. The z-coordinate of a track is measured by the arrival time differences between signals at the individual MWPC wires (time projection). Since the absolute time in respect to the formation of the ionization track is not known, only the inclination of the track with respect to the x, y-plane is measured. The absolute z-position remains undetermined.

In the y-direction the spatial resolution was given by the 16 anode wires of 1 cm spacing. Along the x-direction, several cathode wires were connected together, resulting in a spatial resolution of 10 cm. This resolution was sufficient when compared with the dimensions of the neutron beam of 2–3 cm width (y-direction) and 23 cm length (x-direction), respectively.

The efficiency of the detector for minimum ionizing electrons was determined by a coincidence measurement between the drift chamber and a plastic detector, using a ^{90}Sr beta source [13,16]). An efficiency greater than 95% was measured for single anode wires, corresponding for the given geometry to an ionization track of 1 cm

length in the gas. In the majority of cases several wires are triggered by one event. The probability of observing no signal from an event with a track projection over n anode wires is $(0.05)^n$ and hence the global efficiency very close to 100%.

In our neutron decay measurement the following information was recorded for each event:

(i) anode wire amplitudes;

(ii) anode and cathode time signals with respect to the first fired anode wire;

(iii) time of the first fired anode wire with respect to the time signal from the neutron beam chopper.

5. Admixture of ^{3}He and measurement of the ^{3}He density

A precise knowledge of the ^{3}He content in the counter gas is essential for our method, since the number of neutrons is determined via the ^{3}He (n, p)t reaction (eq. (5)).

The ^{3}He density ρ_0 in the commercial high-purity helium (<1 ppm impurities) was not known and could not be measured with the required accuracy with methods such as mass spectroscopy. To avoid this problem, a well-defined ^{3}He density $\Delta\rho$ was added to the counter gas using 99.999% enriched ^{3}He gas. The number of proton events was measured without and with the additional ^{3}He.

For an identical neutron-flux density the corresponding ^{3}He(n, p)t reaction rate ΔN_p and ΔN_{p_0} are related by

$$\frac{\Delta N_{p_0}}{\Delta N_p} = \frac{\rho_0}{\rho_0 + \Delta\rho}, \tag{7}$$

$$\rho_0 = \frac{\Delta N_{p_0}}{\Delta N_p - \Delta N_{p_0}} \Delta\rho . \tag{8}$$

Eqs. (5) and (8) lead to the following expression for the neutron lifetime, independent of the knowledge of ρ_0:

$$\tau_n^{-1} = \lambda_n = \frac{\Delta N_e}{\Delta N_p - \Delta N_{p_0}} \Delta\rho\sigma(v_0)v_0 . \tag{9}$$

In order not to saturate the detector and the associated electronics by ^{3}He(n, p)t events, the admixture $\Delta\rho$ of ^{3}He must be kept quite low. It can be easily verified that the ^{3}He(n, p) reaction rate is equal to the neutron decay rate for a ^{3}He density of $\sim 3\times 10^{12}$ atoms/cm^3, i.e. 0.1 ppm admixture of ^{3}He at atmospheric pressure. For the commercial helium used, the observed (n, p) reaction rate was three times larger than the neutron decay rate. The admixture $\Delta\rho$ was chosen as $\sim 2\times 10^{13}$ atoms/cm^3 and prepared by expansions between calibrated volumes.

The volume V_1 of the aluminium vessel containing the drift chamber was precisely measured by comparison with a calibrated volume of $V_2 = (25.270 \pm 0.006)$ l. Helium behaves like a perfect gas and corrections are smaller than 10^{-3}. The vessel was

evacuated and then connected to the V_2 volume filled with helium at atmospheric pressure. By measuring, at constant temperature and with high-precision calibrated gauges, the absolute pressures p and p' before and after the expansion, respectively, the volume V_1 was determined as 316.5 ± 0.5 l, using the equation

$$pV_1 = p'(V_1 + V_2) . \tag{10}$$

The admixture of ^{3}He was performed starting with 70 mbar ^{3}He in a calibrated volume $V_3 = 262.66 \pm 0.25$ cm^3. In a first step the gas was expanded into the calibrated volume V_2 which was evacuated before. The volume V_3 was then isolated from V_2 and expanded into the evacuated aluminium vessel V_1. The calibrated volumes were made of clean aluminium walls to limit outgassing and absorption of ^{3}He in the walls. The number of ^{3}He atoms n_1 in the container with volume V_1 and the final ^{3}He density $\Delta\rho$ in the detector vessel are given by the following equations: The initial ^{3}He atoms in V_3 at pressure p_3 and temperature T:

$$n_3 = \frac{p_3 V_3}{kT} , \tag{11}$$

with k the Boltzmann gas constant. In the first expansion:

$$n_{3'} = n_3 \frac{V_3}{V_2 + V_3} , \tag{12}$$

and in the second expansion:

$$n_1 = n_{3'} \frac{V_1}{V_1 + V_3} . \tag{13}$$

The resulting final ^{3}He density in V_1

$$\Delta\rho = \frac{n_1}{V_1} = \frac{p_3}{kT} \frac{V_3^2}{(V_2 + V_3)(V_1 + V_3)} . \tag{14}$$

In the three series of measurements performed (see sect. 6), the ^{3}He density was:

series 1: $1.963\,(5) \times 10^{13}$ atoms/cm^3,
series 2: $1.982\,(5) \times 10^{13}$ atoms/cm^3,
series 3: $1.969\,(5) \times 10^{13}$ atoms/cm^3.

The uncertainties include only the knowledge of the volumes. The additional systematic error in the measurement of pressure, temperature and possible gas absorption or leaks were estimated as $<0.5\%$.

Finally the aluminium vessel V_1, containing now the well-defined amount of ^{3}He, was filled with the counter gas of 70 mbar CO_2 and then 880 mbar of the commercial He. These counter gases were taken from gas bottles at about 100 atm and expanded with needle valves into the aluminium vessel, making diffusion of ^{3}He back into the gas bottles unlikely. Before expansion the commercial helium was passed through a liquid helium cooled trap to clean the gas from possible impurities.

6. Sources of background

For the chosen neutron wavelength of $\lambda = 4.7$ Å only a fraction of 10^{-6} of the neutrons decays within the 70 cm length of the drift chamber. All ionization tracks are detected in the large drift chamber volume with 100% efficiency. Although the three-dimensional reconstruction of the tracks allows a high degree of discrimination of events from the neutron pulse from those of the background (see sect. 7.3), an efficient shielding remained very important.

The ambient background can be classified into two categories: the background which is constant in time and the background correlated with the neutron pulse which is time structured. The ambient background was governed by the natural activity of the material surrounding the drift chamber. The detector was housed in a casemate of 50 cm concrete-wall thickness and surrounded by 5 cm of lead. Due to the 90° deflection of the neutrons out of the primary beam the protection was very effective against the main neutron beam. The presence of the primary beam in the experimental hall contributed only 10% to the total background. Cosmic rays were vetoed by signals from plastic scintillators surrounding the aluminium vessel. For the observed event rates see table 1. No special low-activity materials were used for the detector in this first experiment.

Background events associated with the neutron pulse may occur by neutron capture in the secondary guide, the detector entrance window, gas impurities and in the beam catcher. Furthermore, neutrons are scattered in the detector gas with a probability of 4×10^{-3} per 70 cm and may react with the surrounding materials. This number has to be compared with the neutron decay probability of 10^{-6} while traversing the chamber.

To limit these background events several precautions were taken. The secondary guide was made of 2 mm thick nickel coated glass walls and embedded in $LiCO_3$. The entrance window of the detector was made of 25 μm zirconium which has a low neutron-capture cross section and high mechanical strength. A ^{6}LiF diaphragm in front of the drift chamber absorbed the weak halo of neutrons around the main beam. The entire drift chamber was surrounded by a ^{6}LiF coated plexiglas box, absorbing scattered neutrons and due to its low z-value, limiting the backscattering of decay electrons which leave the drift chamber volume.

TABLE 1

Observed event rates

	Whole detector	Individual anode wire
neutron beam off (cts/s)	100	40
neutron beam on (cts/s)	120	45
neutron beam on with cosmic ray veto (cts/s)	100	30

The neutron-capture probability in the counter gas admixture CO_2 was 1.4×10^{-6} in the 70 cm length of the drift chamber. The most probable direct processes creating charged particles are the internal pair production (IPP) in electromagnetic transitions following neutron capture and the $^{17}O(n, \alpha)^{14}N$ reaction. The IPP with a probability of $\sim 10^{-3}$ per transition and two tracks are insignificant for our purpose. The probability for a $^{17}O(n, \alpha)$ reaction was 6.2×10^{-8} per neutron for the length of the drift chamber and looks like the $^{3}He(n, p)$ events. Impurities of nitrogen would also give rise to events which are not distinguishable from $^{3}He(n, p)$, due to the reaction $^{14}N(n, p)$ with 1.8 b thermal-neutron cross section. Since the neutron density is determined by the *addition* of ^{3}He (see sect. 5), the (n, α) and (n, p) events in the normal counter gas play no role for the evaluation of the neutron lifetime. The proton counting rate was stable within the statistical accuracy and proved that no contamination appeared over the running time of each series of measurements.

7. Measurement and evaluation of the neutron lifetime

7.1. MEASUREMENT SERIES

The neutron lifetime was deduced from three series of measurements performed with the present apparatus. For each run the drift chamber was filled with a new gas mixture. During one week of beam time in total 34 hours of acquisition time were accumulated. The secondary neutron beam was monitored through a small hole in the beam catcher and varied by less than 1% during the measurements. The data were stored in list mode on magnetic tape. The dead time of the acquisition system was 1 ms per event. The evaluation was carried out off-line and will be described in the next section.

7.2. EXTRACTION OF THE $^{3}He(n, p)t$ EVENTS

For a precise evaluation of the neutron lifetime by our method, a perfect discrimination between the neutron decay electrons and the (n, p) events is essential. For this purpose the pulse-height information from the anode wires was used.

The decay electrons can deposit up to 120 keV over the full length of 70 cm of the drift chamber. On the other hand, the range of the protons and tritons from the (n, p) events in the counter gas is 4 and 1 cm, respectively, where most of the available reaction energy of 763 keV is deposited in the last part of the ionization track.

A suitable discrimination parameter was found to be A_{max} defined as the maximum single pulse height among the triggered anodes of each event. This parameter is sensitive to both, length and specific ionization of a track (ref. [16])).

The spectrum of A_{max}, recorded during the presence of the neutron pulse in the drift volume, is shown in fig. 6. The background is already substracted taking events from time intervals, where the neutron pulse is well outside the detector volume.

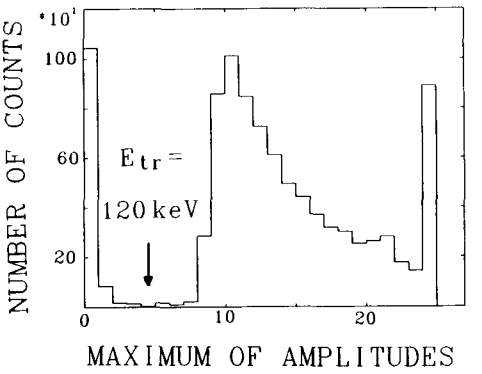

Fig. 6. Pulse-height spectrum for the selected anode, which showed the maximum pulse amplitude among the wires triggered by an event. The energy calibration was performed with α-particles from an ^{241}Am source.

The number of events with intermediate amplitudes (40 to 200 keV energy deposited) is smaller than 1.2% of the main proton bump. Choosing a separation threshold of 120 keV the maximum loss in (n, p) events is estimated as <0.6%.

The event rate above this threshold is plotted against the time-of-flight in fig. 7. The spectrum exhibits a well-defined peak structure corresponding to the passage

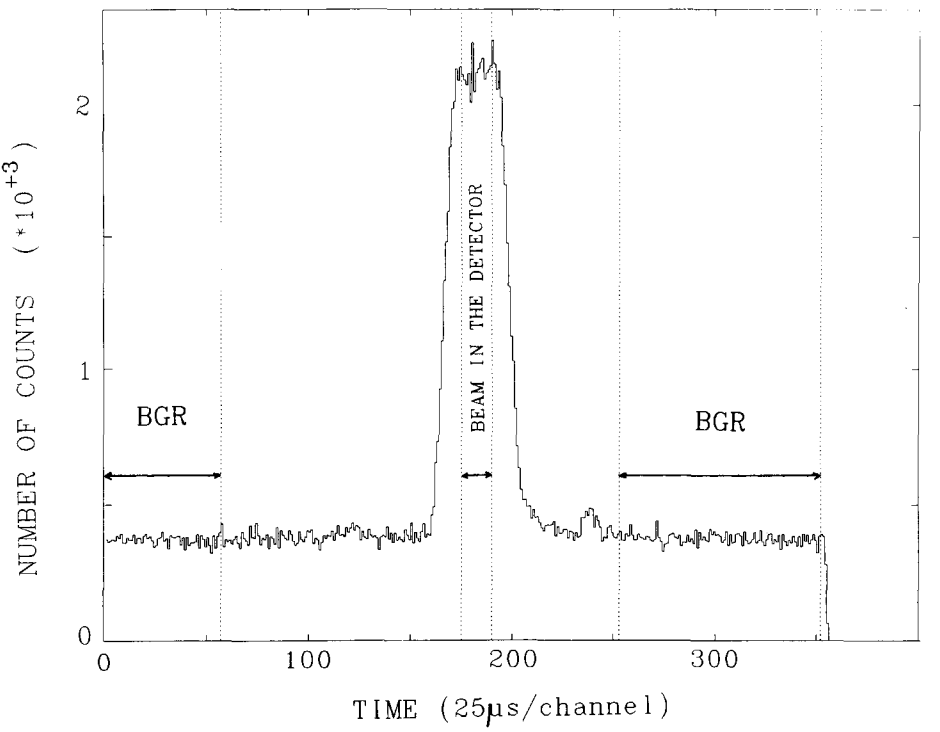

Fig. 7. The (n, p) event rate as a function of time-of-flight of the neutron packet. The background below the peak was estimated from the indicated regions, where the neutron pulse moves outside the drift chamber.

of neutrons through the drift chamber. The flat background probably stems from natural α-activity in the counter gas and from cosmic rays not rejected by the veto signal from the active shielding. The small peak in channel 240 is caused by the reaction of neutrons with the beam catcher.

For the evaluation of the neutron lifetime only the events in the central part of 400 μs of the peak were adopted. The corresponding range is marked in fig. 7 by dotted lines. With a neutron velocity of 837 m/s this time window corresponds to a flight path of 33.5 cm for the neutron pulse of 23 cm length. Thus only those events are taken, which occur well inside the drift chamber, guaranteeing a detection in 4π of solid angle. The background level was taken from the event rate outside the peak. The tails of the proton peak in fig. 7 are associated with events where the neutrons are entering or leaving the drift volume, and reflect also the range of the protons and the lower efficiency of the TPC at the edges.

The (n, p) rates for the individual measurement series are given in table 2. The values are corrected by the dead time of the acquisition system (see the appendix).

7.3. DETERMINATION OF THE NUMBER OF DECAY ELECTRONS

Ionization tracks from electrons are identified as events with maximum of single anode wire amplitudes A_{max} less than 120 keV, according to fig. 6. Using this upper threshold the electron event rate versus time-of-flight of the neutron pulse is shown in fig. 8. Obviously, the spectrum is more difficult to exploit than that of the (n, p) events. Firstly, the peak to background ratio is much less favourable. Secondly, the spectrum exhibits a number of maxima, which can be associated to neutron reactions along the beam line: (1) Neutron capture in the zirconium entrance window of the detector vessel, (2) ^{6}LiF collimator, (5) ^{6}LiF beam catcher. Thirdly, the neutron decay electron peak seems to sit on a broad bump which can be attributed to the diffusion of neutrons in the counter gas followed by neutron capture in the surrounding materials. This effect was reduced by surrounding the drift chamber by a ^{6}LiF coated box (see sect. 6).

Because of all these difficulties further data reduction was necessary in order to evaluate the neutron beta decay rate.

In a first step the tracks were corrected for missing triggers of wires. With a detection efficiency of $\geqslant$95% per wire the probability for missing a trigger for a track over M wires is $\leqslant(1\text{-}0.95)^M$. For about 10% of the observed tracks a trigger within well correlated track points was missing, in accordance with the estimation. For further evaluations these missing points were filled up.

Next the distribution of the number of fired anode wires, called "multiplicity" in the following, was investigated for the ensemble of electron events. In fig. 9 the multiplicity distribution for background events is shown, i.e. for the case of the neutron pulse being outside the chamber. This experimental finding is compared with a Monte Carlo simulation, where an isotropic electron irradiation from outside

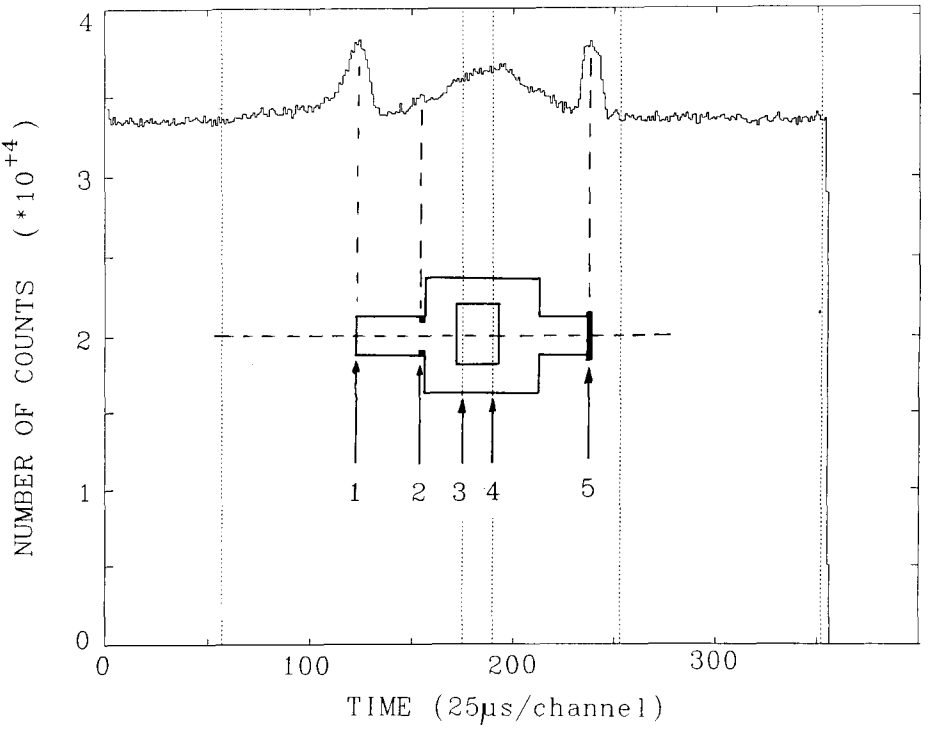

Fig. 8. Same as fig. 7, but for electron events without any cut in the data. The position of the neutron packet with respect to the detector is shown schematically. Entrance window (1), ^{6}LiF collimator (2), neutron beam fully in the detector (3, 4) and beam catcher (5).

the drift chamber is assumed. The simulation reproduces well the data for multiplicities ≥ 3. For lower multiplicities an excess of events is observed, which may be due to low energy X-rays or electronic noise. In addition, it was found that the ^{6}LiF layer surrounding the drift chamber was weakly radioactive producing low-multiplicity events, probably due to tritium contamination from former use of the material in neutron beams.

For neutron decay electrons originating from the center of the drift chamber, a multiplicity in the range from 4 to 8 is expected for the major part of the events [see ref. [16]) and fig. 17 below]. Again an excess of multiplicities 1 and 2 was observed. A possible explanation is based on a secondary effect from neutron capture in CO_2 or on small hydrocarbon contamination in the counter gas. As discussed in sect. 6 the nuclear radiation itself, following the neutron capture in CO_2, should not have any visible effect. But the nuclear recoil in the (n, γ) reaction may break the chemical bond followed by UV irradiation. This effect was more pronounced when we replaced the CO_2 quenching gas by CH_4. Due to the higher neutron capture cross section of hydrogen the capture rate was increased by about a factor of 390. A large rate of low multiplicity events was observed, correlated in time and space with the neutrons. The observed rate of these events was compatible with an 80% efficiency for detecting

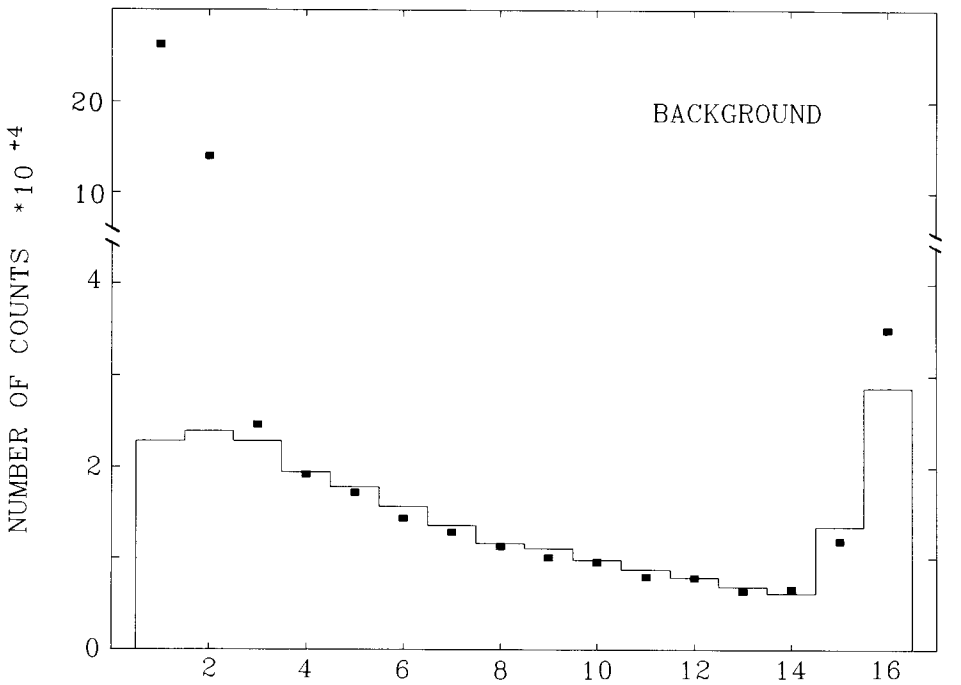

Fig. 9. Observed multiplicity distribution for the background (points) compared with the Monte Carlo simulation (histogram).

the deuterium recoil from the reaction p(n, γ)d. The time spectrum of $M = 1$ events observed for individual anode wires is shown in fig. 10 for the case of the usual CO_2 quenching gas.

Because of these problems we disregarded events with multiplicity 1 and 2. The associated losses for neutron decay electrons were calculated by a Monte Carlo simulation, taking into account:

(i) neutron packet displacement in the drift chamber;

(ii) spatial distribution of the neutron packet;

(iii) energy distribution of the decay electrons;

(iv) multiple scattering of the decay electrons in the counter gas.

The losses due to the elimination of the multiplicities 1 and 2 were calculated as $(11 \pm 1\%)$.

In fig. 11 the observed multiplicity distribution for the events $M \geq 3$ correlated with the presence of the neutrons in the drift chamber is shown. The background taken from the time intervals without neutrons in the chamber is already subtracted. The data are compared with a Monte Carlo calculation of neutron beta decay events. The observation of multiplicities higher than 8 indicates that an additional background component is under the neutron decay events.

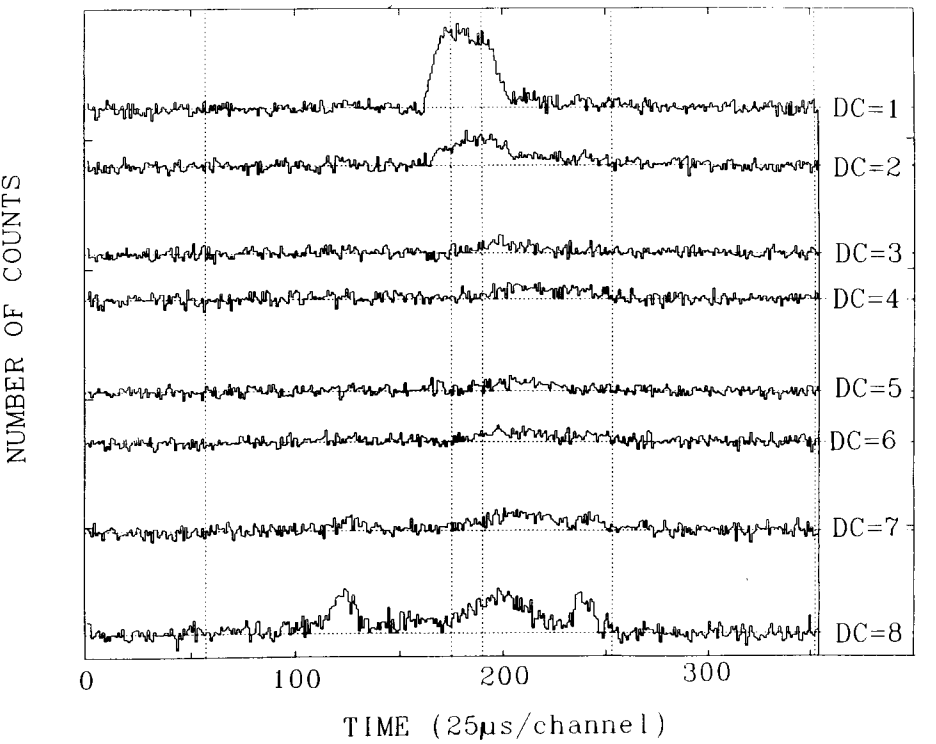

Fig. 10. The time spectra of $M = 1$ events observed for anode wires. Each spectrum corresponds to the data collected on two wires equally distant from the neutron beam axis (parameter DC in cm).

In the next step of the evaluation, tracks which traverse the whole drift chamber were rejected since they correspond obviously to background events. In the z-direction those events may show a large drift-time difference between the first and last anode wire fired. According to fig. 12a the maximum drift time measured for background events was 24 ± 2 μs. Including the spatial spread of the neutron burst, the maximum drift-time difference in decay electron tracks should not exceed 16 μs (fig. 12b) and thus events with >16 μs were rejected from the data set. In the x-direction events were rejected when both the first and last cathode are triggered. These events correspond to background from outside passing the drift volume along the neutron beam direction. The time spectrum of the eliminated events are shown in fig. 13.

In the remaining data the time structure in the background and in particular the bump below the neutron decay electrons were still visible as shown for individual anode wires in fig. 14. Thus it was not allowed to take the background under the neutron decay events from time intervals, where no neutrons are present in the detector.

For further investigation of the background we compared the events from different parts of the detector. Fig. 14 shows the time spectra for events originating at different

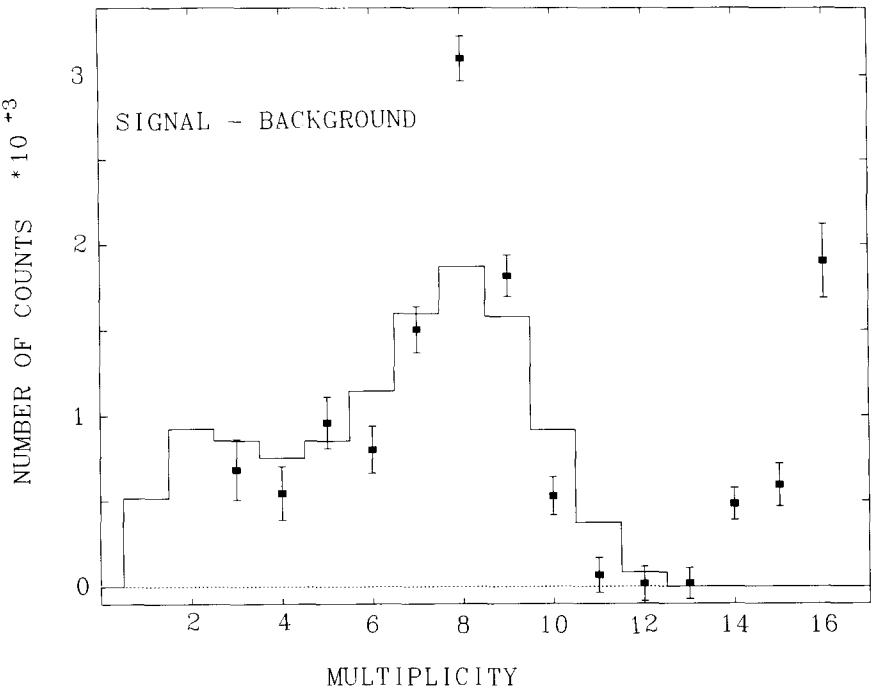

Fig. 11. Multiplicity distribution for the events correlated with the neutron packet in the drift chamber. Here the subtracted background is taken from regions where the neutron pulse is well outside the detector. The Monte Carlo calculation is shown by the histogram.

distances from the center of the drift chamber in y-direction. For this purpose the two extreme points of a track were determined and their distances to the neutron beam axis calculated. The minimum between these two distances is defined as the parameter DC. The precise location and width of the neutron beam was measured with multiplicity $M = 1$ events and is shown in figs. 10 and 15. The neutron beam is centered between anode wire 7 and 8 and its full width is within the wires 6, 7, 8, 9 (DC = 1, 2).

For the events with DC = 1, 2 the remaining background contributions are shown schematically in fig. 16, assuming that the background originates from outside the drift volume and taking into account already the elimination of events with maximum drift time difference >16 μs and those triggering the first and last cathode. The tracks entering or leaving the chamber through the shadowed areas cannot be discriminated from neutron decay events, since we are not able to determine the absolute z-values for a track. The background for other parts of the detector should be quite similar as long as one remains close to the center. As the final neutron beta decay event rate we have adopted the difference between DC = {1, 2} and DC = {3, 4, 5}. The background level was normalized to the time interval where no neutrons are present in the chamber.

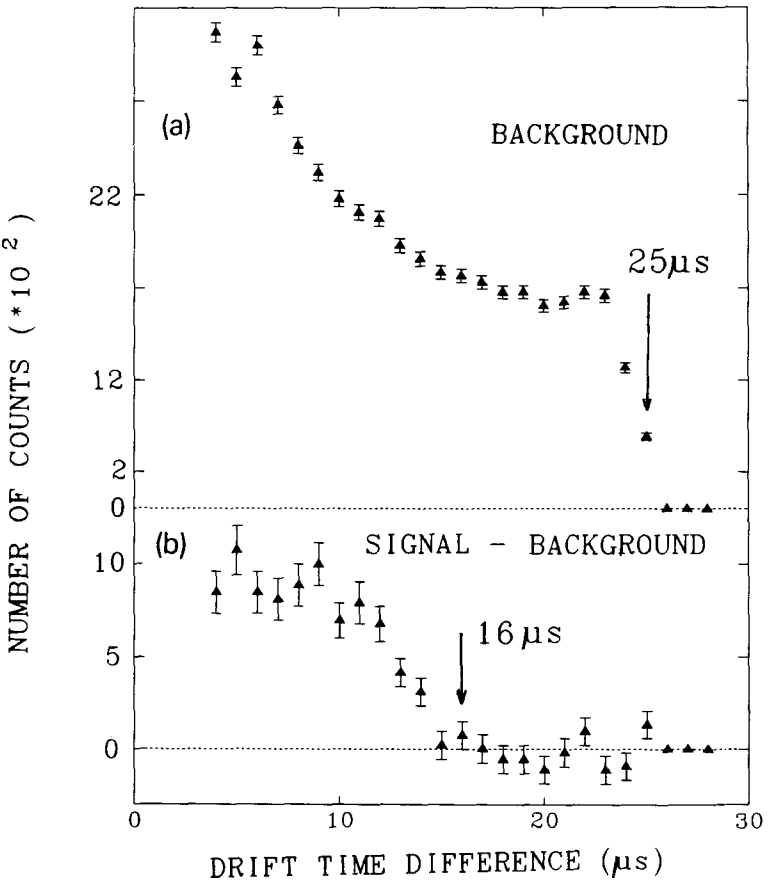

Fig. 12. Distribution of the maximum drift-time difference for electron tracks: (a) background events, (b) neutron decay events.

A small correction to that neutron decay event rate may be necessary due to the efficiency of the drift chamber for electrons. The neutron beam is well within the limits for DC = 1, 2 as can be seen from figs. 10 and 15. The full beam width spreads from the exit of the neutron guide of 15 mm to the width of 60 mm at the beam catcher (fig. 4). The drift chamber is placed in the middle and thus the beam in the drift chamber has about 30 mm full width. Nevertheless an electron track starting in DC = 2 may only be detected first in DC = 3. The probability of this effect is related to the length of the ionisation track deposited in DC = 2 and the associated efficiency of the chamber. As already mentioned the efficiency was measured with minimum ionising electrons as $\geqslant$95% per 1 cm length of the ionization track [16]). Half of the tracks starting in DC = 2 leave towards DC = 3, i.e. about 12% of all neutron decay events (see fig. 10). Most of those tracks are inclined and thus deposit a sufficiently long ionization path in DC = 2 to be detected with almost 100% efficiency. Thus, losses of neutron decay events in our evaluation due to DC = 3

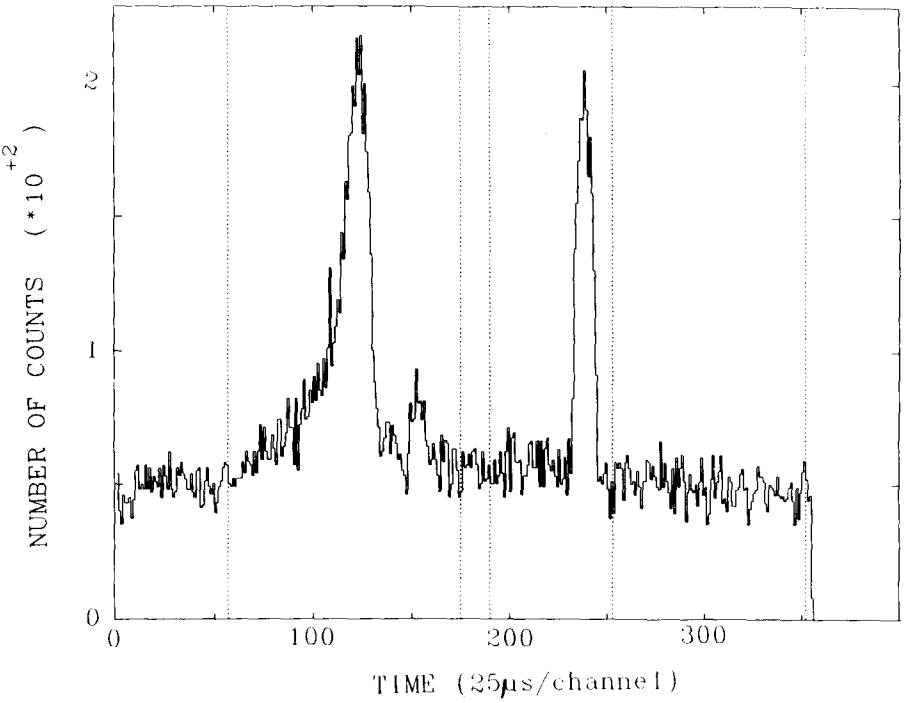

Fig. 13. Events eliminated by the condition that a neutron decaying inside the drift volume should not trigger both the first and last cathode. The three peaks in the spectrum corresponds to the passage of the neutrons through the entrance window, the ^{6}LiF diaphragm and the absorption in the beam catcher, respectively.

detection should be small. An estimate of the effect can be obtained by comparing (i) DC{1, 2} − DC{3, 4, 5} × norm with (ii) DC{1, 2} − DC{4, 5}. For the case (i) neutron decay events Δ_3 detected at DC = 3 would cause a correction of $\Delta_3 + \Delta_3 \times$ norm, with the normalization factor, norm, $\sim\frac{2}{3}$. For the case (ii) the correction is only Δ_3. We have measured the difference $\Delta_3 \times \frac{2}{3}$ between the two evaluations as +0.35%, which is statistically not significant. Since this possible systematic error can only yield a shorter neutron life time, we adopted a correction of $\Delta_3 \times \frac{5}{3} = 0.9\%$ on our neutron decay event rate and an error of the same magnitude.

Some neutron decay electrons originating from the center of the detector are backscattered by the surrounding materials. Using low-Z materials this effect is reduced (see sect. 6). A backscattered decay electron may then pass through the detector volume again and thus create a high-multiplicity track. For some cases the origin DC = 1, 2 of the track can no longer be identified and thus the event is not recorded as a neutron decay electron. The associated losses are small and were estimated by a measurement with a ^{204}Tl beta source placed in the center of the detector. The measured multiplicity distribution is given in fig. 17. The excess in multiplicities higher than 10 amounts to 1.5 ± 0.5% and was attributed to backscattering. The activity of the ^{204}Tl source was known with a precision of 2%. Our measured

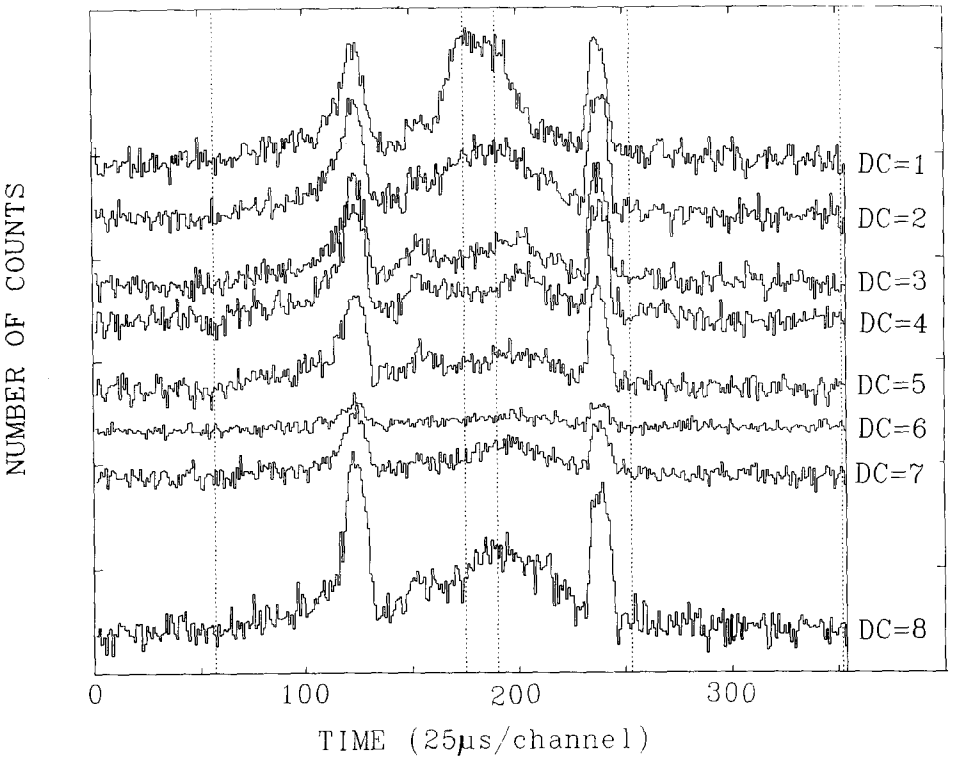

Fig. 14. Time spectra of electron events selected by the closest distance of the track to the center of the neutron beam axis (parameter DC in cm).

event rate agreed perfectly with the given activity when including the backscattering events [16]).

In fig. 18 the time spectra for the events with DC = {1, 2} and the normalized background from DC = {3, 4, 5} are compared. They show the same time structure, which gives us confidence that this type of background definition is correct. Thus the time structure of the background and the track identification allows us to determine the background during the presence of the neutrons in the drift volume.

Fig. 19 shows a magnified view of the neutron decay peak after the background subtraction. The spectra of the three measurement series are given (fig. 19a) as well as the cumulated data (fig. 19b).

8. Evaluation of the neutron lifetime

Table 2 summarizes the data and results for the three measurement series. For each run two different gas mixtures were prepared with normal helium and additional ^{3}He content, respectively. The measurement with high ^{3}He content covered about 15% of the acquisition time and aimed mainly at the measurement of the (n, p) event rate. There is no systematic difference between the deduced decay electron rate for the different ^{3}He contents proving the good separation between electron and (n, p) events.

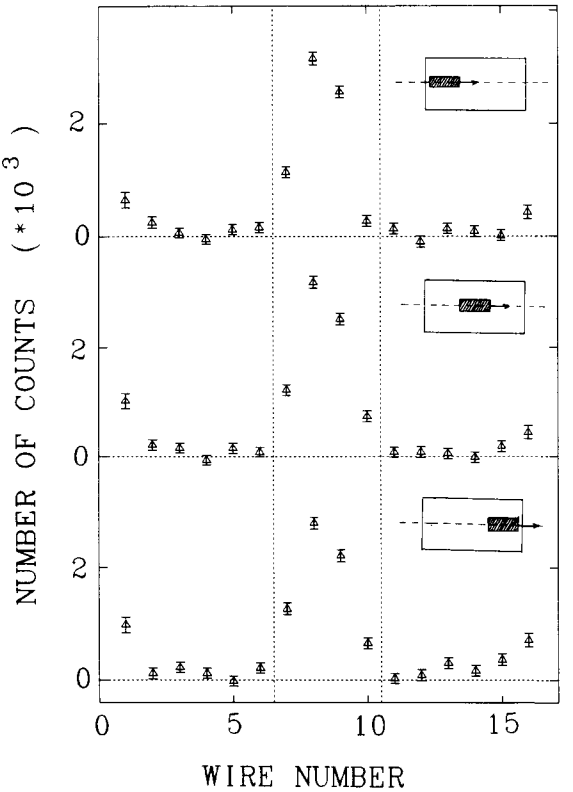

Fig. 15. Beam spread in horizontal direction measured by multiplicity $M = 1$ events in the drift chamber. The spectra (background subtracted) correspond to three different positions of the neutron packet. The increase of the beam divergence over the detector length is small.

TABLE 2

Summary of the data for the evaluation of the neutron lifetime. The counting rates are already dead-time corrected.

	Series 1		Series 2		Series 3	
	normal ^{3}He	added ^{3}He	normal ^{3}He	added ^{3}He	normal ^{3}He	added ^{3}He
$\Delta N_e(s^{-1})$ [a]	1.768 ± 0.095	0.94 ± 0.32	1.745 ± 0.111	2.02 ± 0.24	1.968 ± 0.100	1.75 ± 0.24
mean $\Delta N_e\,(s^{-1})$ [a]	1.699 ± 0.091		1.794 ± 0.102		1.936 ± 0.092	
F	$(5.91 \pm 0.09) \times 10^{-4}$		$(5.44 \pm 0.05) \times 10^{-4}$		$(5.15 \pm 0.05) \times 10^{-4}$	
$\lambda_n' = F\Delta N_e\,(s^{-1})$ [b]	$(1.004 \pm 0.056) \times 10^{-3}$		$(0.976 \pm 0.056) \times 10^{-3}$		$(0.997 \pm 0.049) \times 10^{-3}$	

mean value $\bar{\lambda}_n'(s^{-1})$ $(0.9927 \pm 0.0308)10^{-3}$
correction factor for cut in multiplicity 1.12 ± 0.01
correction factor for backscattering 1.015 ± 0.005
possible losses in DC = 3 events 1.009 ± 0.009
$\lambda_n = \bar{\lambda}_n' \times$ correction factors (s^{-1}) $(1.139 \pm 0.039) \times 10^{-3}$
$\tau_n = \dfrac{1}{\lambda_n}(s)$ 878 ± 31 s

[b] $F = (\Delta N_p - \Delta N_{p0})^{-1} \Delta\rho\sigma(v_0)v_0$ (see eq. 9).
[a] ΔN_e, ΔN_p in counts per second during 400 μs, when the neutron packet moves inside of the detector.

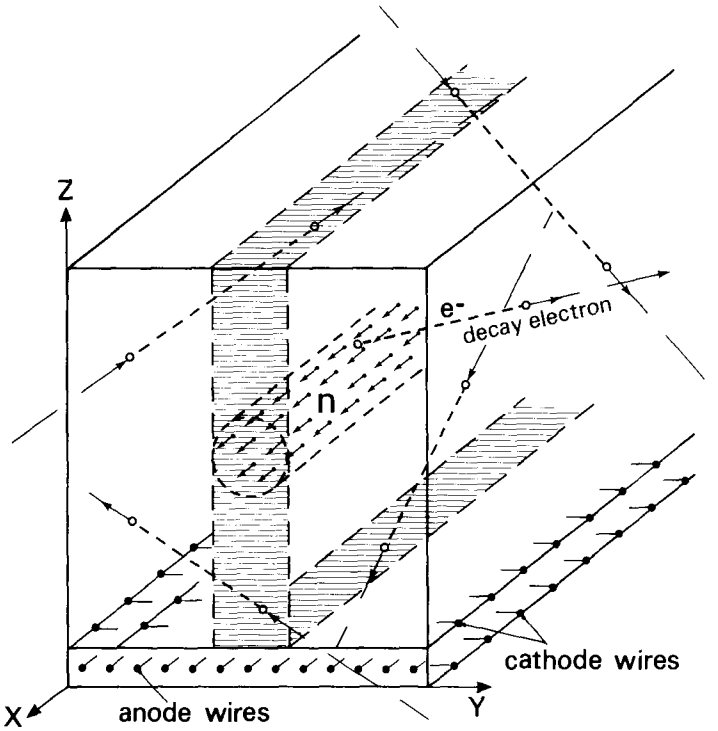

Fig. 16. Possible trajectories of electrons which contribute as indistinguishable background to the neutron decay events, even when only events with DC = 1, 2 and those not triggering the first and last cathode together are selected.

The individual neutron lifetime values were derived by putting the given values into eq. (9).

The errors in the (n, p) and decay-electron rates are governed by statistical uncertainties. The global systematic error of 1.6% due to the multiplicity cut (1%), the separation of electron and (n, p) events (0.6%), backscattering correction (0.5%) and the correction due to possible DC = 3 events (0.9%) is added below to the final error. The errors in $\Delta\rho$ take into account the uncertainties in the pressure, temperature and, as global error, the calibrated volume measurements. The error of $\sigma(v_0)$ is negligibly small at the present level of precision. As shown in sect. 6 gas contamination plays no role in the determination of τ_n. For the determination of the background no systematic error is visible within the present statistical accuracy. With all these corrections and uncertainties we derive as final value for the free neutron lifetime (see fig. 1)

$$\tau_n = 878 \pm 31 \text{ s}$$

The uncertainty is composed of 27 s statistical error, and 14 s systematic error, added quadratically.

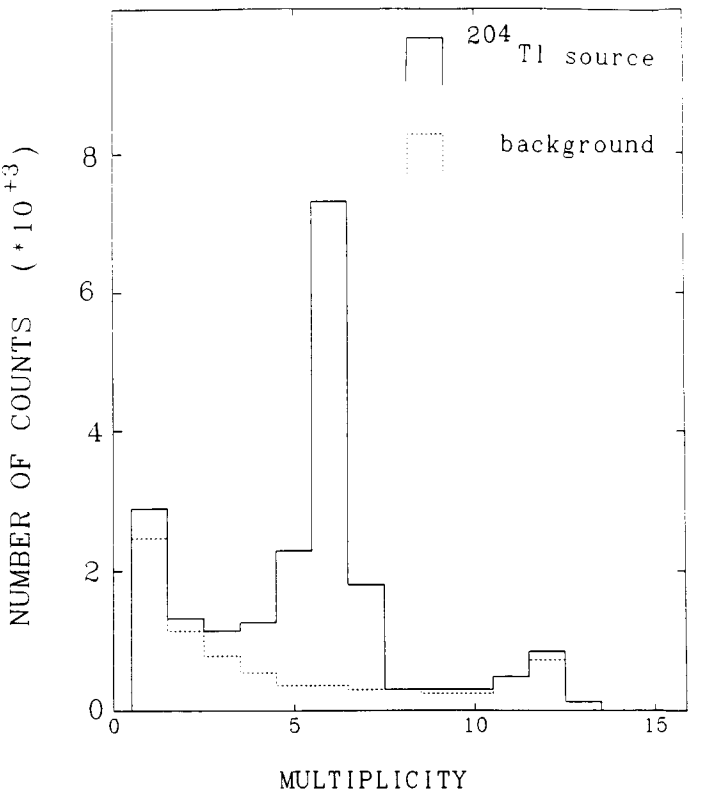

Fig. 17. Multiplicity distribution for electrons from a ^{204}Tl beta source placed in the center of the detector. The excess in high multiplicity events is attributed to backscatterng from surrounding materials.

9. Conclusion and outlook

In previous neutron beam experiments the lifetime of the free neutron was deduced from the *separate* measurements of the decay particles (electrons or recoil protons) and the number of neutrons which may undergo the decay. In the novel method presented in this paper the value of the neutron lifetime was obtained by a *relative* measurement, namely the ratio of decay electrons to protons from the ^{3}He(n, p)t reaction, where the particles were measured in the same detector. The solid angle for the detection of both particles was 4π for neutron pulses moving inside of the detector. The energy threshold for the decay electrons was of the order of a few keV and associated losses negligible. Thus, a number of possible systematic errors due to detector dead-time corrections, beam profile, energy spectrum of decay products, decay volume definition etc. were avoided.

The background in the present measurement was investigated in much detail, and its level was determined dynamically with the chopped neutron beam. The track reconstruction of the events allowed us to measure the additional background which

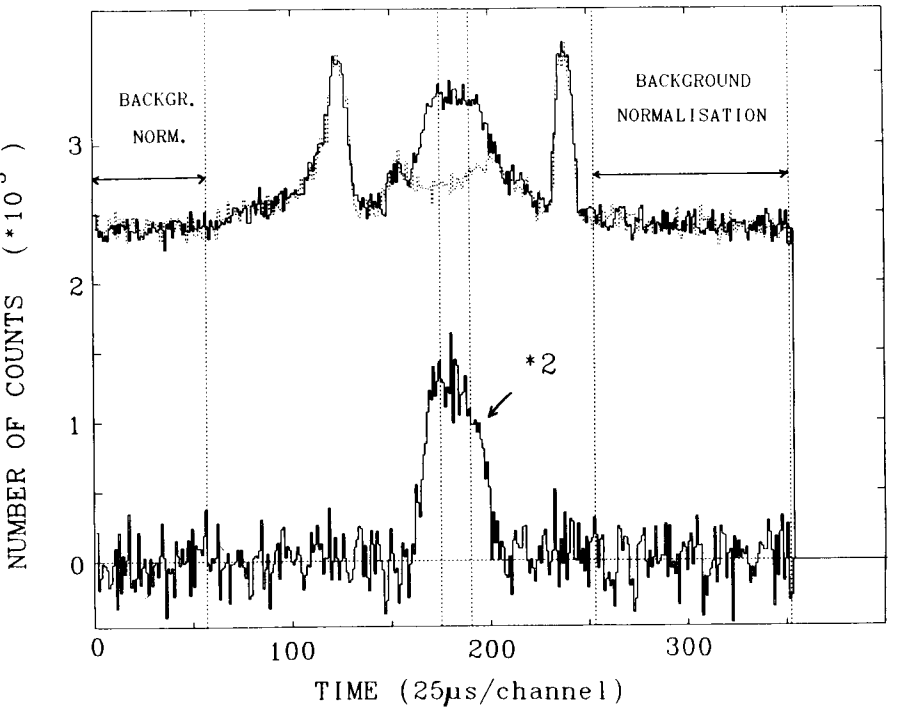

Fig. 18. Time spectra for selected electron events with DC = {1, 2} (solid line) and DC = {3, 4, 5} (dashed line). The DC = {3, 4, 5} spectrum was normalized to match the DC = {1, 2} spectrum in the regions indicated. The difference between both spectra is shown in the bottom of the figure.

is caused by the presence of the neutron pulse in the detector vessel. This background component was an ambiguity in previous neutron beam experiments.

In the first measurement presented here we obtained a value for the neutron lifetime of $\tau_n = 878\,(31)$ s. The precision was mainly limited by the statistical accuracy, achieved in the available short beam time.

For the future various improvements of the method are foreseen apart from a longer acquisition time. Firstly, the neutron beam intensity can be significantly increased using a graphite monochromator of better reflectivity together with a focussing beam geometry. A better signal to background ratio could be obtained when using low-activity materials for both the detector and shielding. The detector vessel will be cladded with graphite to absorb the beta particles from neutron capture and γ-absorption in the aluminium walls (graphite has a low neutron capture cross section of only 3.5 mb and a low γ-absorption coefficient).

A major part of the background could be eliminated if the absolute-z coordinate of the ionization tracks could be determined. This could be accomplished by surrounding the drift chamber volume by separate MWPC planes. For electrons

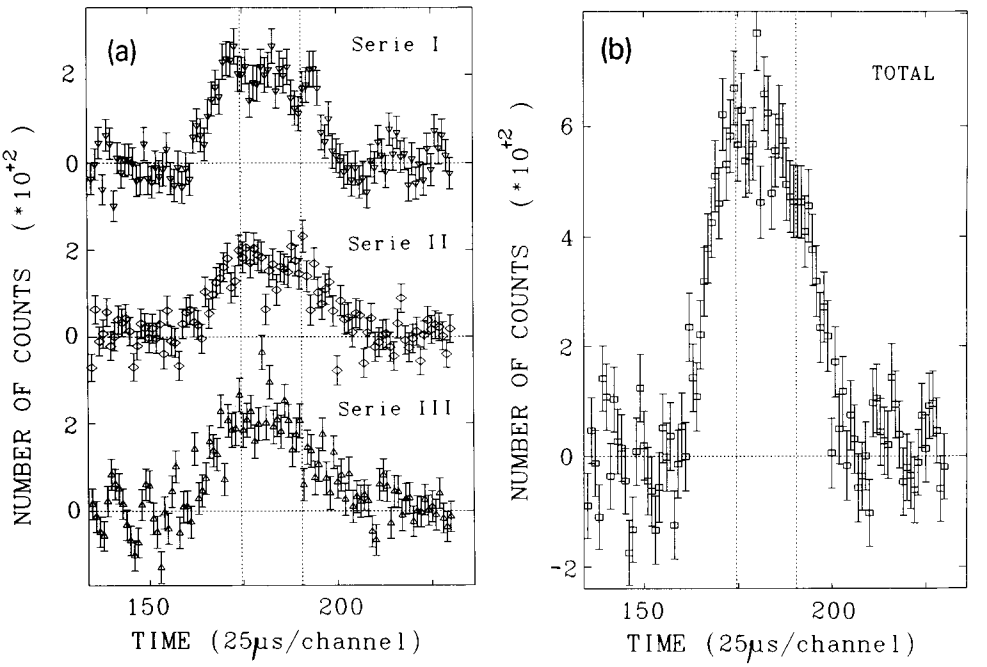

Fig. 19. Magnified view of the observed electron signal: (a) for each acquisition series; (b) cumulated spectrum.

triggering both the TPC and a MWPC plane the time zero given by the MWPC would allow an unambiguous reconstruction of the track in the TPC. According to fig. 16 the most important MWPC planes are those which are parallel to the xy plane, since most of background tracks shown in fig. 16 would pass through them. The triggers from these two wire planes provide already an absolute-z localization for tracks from the center of the drift volume and thus an efficient background rejection. In addition those two wire planes would offer a better analysis of the low-multiplicity events. In the present experiment the major part of the low-multiplicity background seems to originate from point-like ionization events. They would not trigger both the TPC and the additional MWPC and hence could be discriminated against the neutron decay electrons which are in general energetic enough to leave the drift volume and trigger the MWPC. Thus the multiplicity cut $M \geq 3$ may no longer be necessary.

With these improvements a statistical accuracy of better than 1% should be feasible in a few weeks of beam time. The ultimate limit for the precision in τ_n will then be given by systematical uncertainties, in particular by the precision to which the efficiency and the background of the detector can be determined.

Finally, the present drift chamber can be easily adapted for a measurement of the beta decay asymmetry of polarized neutrons, the coefficient A. With a neutron polarization in the y-direction and plastic scintillators on both sides of the TPC the decay electrons of interest could be measured in coincidence between the gas detector and the scintillator. The scintillator would provide the energy of the electrons and the time-zero trigger for the absolute determination of the z-coordinate in the TPC. A full reconstruction of the ionization track in the TPC is possible and facilitated by the high multiplicity (half of the anode wires) of the events of interest. Thus a precise measurement of the energy and emission angle of decay electrons from polarized neutrons is feasible under favorable background conditions.

We acknowledge the financial support of the Institut Laue-Langevin as well as the continuous effort of its technial staff. In particular, we thank G. Blanc and P. Ledebt who helped us with mechanical construction and data acquisition, respectively. The technical staff of the Institut des Sciences Nucléaires de Grenoble has been of great efficiency; we are specially indebted to J. Ballon who took in charge the construction of the drift chamber and B. Guerre-Chaley who built an important part of our electronic setup. The Laboratoire de Physique des Particules d'Annecy which supplied numerous electronic devices is also acknowledged. We thank A. Bussière, J. Chauvin and P. De Saintignon who participated in the early stage of the experiment. We also thank the students G. Klees and B. Hugues for computing Monte Carlo simulations for the experiment.

Appendix

CORRECTION FOR THE ACQUISITION DEAD TIME

In principle no dead-time correction would be necessary with the present method, if both the decay-electron events and (n, p) events are measured simultaneously and background free. However, we have recorded the relevant (n, p) events at a higher ^{3}He admixture and hence somewhat higher total event rate than during the main decay-electron measurements. Also a dead-time correction term enters by the subtraction of the background.

During the passage of the neutron beam through the detector the counting rate is higher and the dead time more important. Thus the recorded counting rate of the background events in the detector is reduced during this time interval and the background subtraction must take into account this effect.

The dead-time-corrected rate per time unit is given by

$$\Delta N_i = \frac{1}{\Delta t_1}\int_{\Delta t_1}\frac{dN_i(t)}{dt}f(t)\,dt - \frac{1}{\Delta t_2}\int_{\Delta t_2}\frac{dN_i(t)}{dt}f(t)\,dt,$$

where Δt_1 and Δt_2 are the time intervals with the neutron packet inside the drift volume and well outside, respectively. The function $f(t)$ denotes the dead-time correction, $N_i(t)$ the recorded events with i electron or proton type.

The ratio $R = \Delta N_e / \Delta N_p$ enters then in the formula (9) of the neutron lifetime evaluation. Obviously for a constant dead time function $f(t) = \text{const.}$ the ratio R would not be influenced by this correction.

The dead time is now composed of the following contributions:

- T_{acq} acquisition dead time ~1 ms/event,
- T_{tr} transfer dead time from the computer memory to the magnetic tape: 500 ms/transfer of 200 events,
- T_{cos} dead time caused by the veto signal from the cosmic ray shielding: 50 μs/veto signal.

The first listed component depends on the position of the neutron beam packet, i.e. on the time structure of the event rates. The two other components are randomly distributed.

The probability that the detector is blocked at the instant t during an acquisition period is given by

$$P(t) = \frac{1}{N_{cyc}} \left(\int_{t-T_{acq}}^{t} dN_{ev} + \frac{T_{tr}}{T_{cyc}} \frac{N_{ev}}{200} + \frac{T_{cos}}{T_{cyc}} N_{cos} \right),$$

where N_{cyc} is the number of chopper cycles during the acquisition period; N_{ev} the number of collected events during the acquisition period; N_{cos} the number of cosmic ray vetos during the acquisition period; and T_{cyc} the period of one chopper cycle.

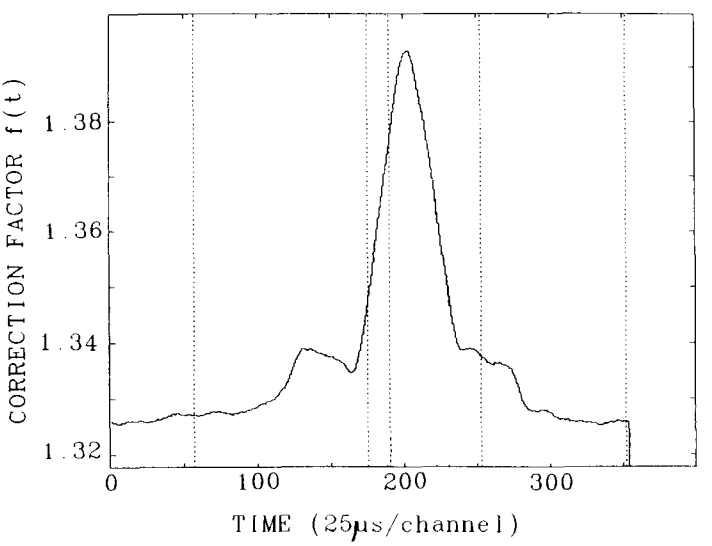

Fig. 20. Beam position dependent correction factor for the acquisition dead time.

The dead-time correction factor $f(t)$ is given then by

$$f(t)=\frac{1}{1-P(t)}$$

In fig. 20 a typical form of the function $f(t)$ is shown. All the time spectra in this paper are corrected for the effect. The dead-time correction for the value R was of the order of 2%.

References

1) Particle Data Group: Review of Particle Properties, Phys. Lett. **B204** (1988) 1;
D.H. Wilkinson, Nucl. Phys. **A377** (1982) 474
2) A. Sirlin, Phys. Rev. **D35** (1987) 3423
3) L.A. Mikaelyan, M.D. Shorokhvatov and A.V. Etenko, in 'Neutrino 88', ed. J. Schneps *et al.* (World Scientific, Singapore, 1989) in press
4) G. Zacek *et al.*, Phys. Rev. **C34** (1986) 2621;
J. Bouchez, in 'Neutrino 88', ed. J. Schneps *et al.* (World Scientific, Singapore, 1989) in press and references cited therein
5) J. Byrne, J. de Phys. **C3** (1984) 31
6) C.J. Christensen, A. Nielsen, A. Bahnsen, W.K. Brown and B.M. Rudstad, Phys. Rev. **D5** (1972) 1628
7) L.N. Bondarenko, V.V. Kurguzov, Yu. A. Prokofiev, E.V. Rogov and P.E. Spivak, JETP Lett. **28** (1978) 303
8) J. Byrne, J. Morse, K.F. Smith, F. Shaikh, K. Green and G.L. Greene, Phys. Lett. **B92** (1980) 274
9) Yu. Yu. Kosvintsev, V.I. Morozov and G.I. Terkhov, JETP Lett. **44** (1986) 571
10) J. Last, M. Arnold, J. Döhner, D. Dubbers and S.J. Freedman, Phys. Rev. Lett. **60** (1988) 995
11) K.J. Kügler, K. Moritz, W. Paul and U. Trinks, Nucl. Instr. Meth. **A228** (1985) 240
12) P. Ageron, W. Mampe, J.C. Bates and J.M. Pendlebury, Nucl. Instr. Meth. **A249** (1986) 261;
W. Mampe, in The investigation of fundamental interactions with cold neutrons, ed. G.L. Greene (NBS Special Publication 711, Washington 1986) p. 59
13) P. Liaud, K. Schreckenbach, J. Chauvin, P. de Saintignon and A. Bussière, J. de Phys. **C3** (1984) 37
14) S.F. Mughabhab, M. Diradeemam and N.E. Holden, Neutron cross sections, vol. 1 (Academic Press New York, 1981)
15) J. Als-Nielsen and O. Dietrich, Phys. Rev. **133** (1964) B925
16) P. Grivot, R. Kossakowski, P. Liaud, K. Schreckenbach, G. Azuelos, A. Bussière and P. de Saintignon, Nucl. Instr. Meth. **B34** (1988) 127
17) A. Bussière, J. Chauvin, P. Grivot, R. Kossakowski, P. Liaud, P. de Saintignon and K. Schreckenbach, J. of Phys. **E21** (1988) 1183